

doi:10.15199/48.2019.06.05

## Analysis of Epstein frame by Finite Element Method

**Abstract.** An Epstein frame has been built, which is used to measure magnetic properties of different kind of cores. Sinusoidal voltage excitation has been used in a frequency range of 1-400Hz. The measurements have been performed by a computer-controlled measurement system. The building and the measurement process have been published before. The objective of this work is to compare the simulation results performed with the COMSOL Multiphysics build-in modules and some potential formulation. For this work the Jiles-Atherton model has been chosen to prescribe hysteresis phenomena. The model parameters can be obtained by using the measurement results. The frame has been modelled in 2D.

**Streszczenie.** W artykule zaprezentowano analizę systemu wykorzystującego platformę COMSOL Multiphysics. Użyto modelu Jiles-Atherton do opisu histerezy. Przeprowadzono analizę 2D wykorzystując parametry uzyskane doświadczalnie. **Analiza satemu Epsteina z wykorzystaniem metody elementów skoczonych**

**Keywords:** Epstein frame, COMSOL Multiphysics, Jiles-Atherton model, Finite Element Method, Potential formulation

**Słowa kluczowe:** metoda Epsteina, platforma COMSOL Multiphysics, metoda elementów skoczonych.

### Introduction

The previous work was to build up an Epstein frame. The measurement results and the implementation of the Jiles-Atherton hysteresis model into COMSOL Multiphysics have been published in [20].

The objective of this work is to compare computational time using COMSOL Multiphysics with different techniques. The main goal is to reduce the software simulation time as much as possible while the accuracy of the results should not decrease. The Epstein frame has been modelled in 2D.

These results will be used later in Linear Parameter Varying (LPV) [3, 16] modelling of the frequency and temperature properties of an induction machine [8, 11, 14, 19].

### The Epstein frame

The Epstein frame is used to measure magnetic properties of electrical steels [4, 10, 12, 18]. The building and measuring process have been published [20]. The measurements have been performed analysing the material M250-35A produced by the ArceroMittal. During measurements, current excitation has been applied with a control mechanism to obtain sinusoidal induced voltage and magnetic flux density. Measurements have been performed applying 7 different frequencies with 8 different amplitudes. Fast Fourier Transform (FFT) have been used where every harmonic component have been removed. These filtered excitation signals have been used during the simulations, too. In Fig.1. the completed frame can be seen.

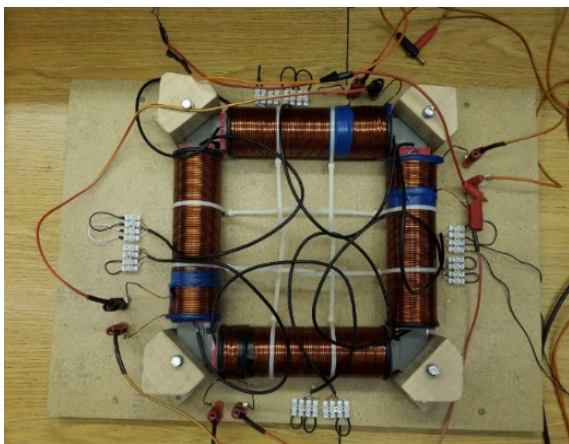


Fig.1. The measurement ready Epstein frame

### The Jiles-Atherton model

While measuring ferromagnetic materials, hysteresis phenomenon can be observed [1, 2, 9, 13, 15]. For this work, the Jiles-Atherton hysteresis model has been chosen. The necessary formulas can be found in [6, 7, 17]. The following equations have been implemented into the frame of COMSOL Multiphysics:

$$(1) \quad \mathbf{B} = \mu_0 (\mathbf{H} + \mathbf{M}),$$

$$(2) \quad \mathbf{M} = \mathbf{M}_{rev} + \mathbf{M}_{irr},$$

$$(3) \quad \mathbf{M}_{rev} = c(\mathbf{M}_{an} - \mathbf{M}),$$

$$(4) \quad \mathbf{M}_{rev} = \frac{c}{1-c}(\mathbf{M}_{an} - \mathbf{M}_{irr}),$$

$$(5) \quad \mathbf{H}_e = \mathbf{H} + \alpha \mathbf{M},$$

$$(6) \quad \mathbf{M}_{an} = M_s \left( \coth \frac{|\mathbf{H}_e|}{a} - \frac{a}{|\mathbf{H}_e|} \right) \frac{\mathbf{H}_e}{|\mathbf{H}_e|},$$

$$(7) \quad \frac{\partial \mathbf{M}_{irr}}{\partial t} = g \left( \frac{\mathbf{M}_{rev}}{ck} \cdot \frac{\partial \mathbf{H}_e}{\partial t} \right) \frac{\mathbf{M}_{rev}}{|\mathbf{M}_{rev}|}; g(x) = \begin{cases} x & x \geq 0 \\ 0 & x < 0 \end{cases}$$

where  $\mathbf{B}$  is the magnetic flux density,  $\mathbf{H}$  is the magnetic field intensity,  $\mathbf{M}$  is the magnetization of the core,  $\mu_0$  is the permeability of vacuum, the *rev* subscript means reversible part, *irr* signs for irreversible part of magnetization,  $\mathbf{M}_{an}$  is for the anhysteretic magnetization,  $\mathbf{H}_e$  is the so-called effective field, finally  $a, \alpha, c, k, M_s$  are the model parameters.

The partial differential equation of the Jiles-Atherton model can be formulated as

$$(8) \quad \frac{\partial \mathbf{M}}{\partial t} = (1-c) \frac{\partial \mathbf{M}_{irr}}{\partial t} + c \frac{\partial \mathbf{M}_{an}}{\partial t}.$$

The implementation of (1)-(8) into COMSOL Multiphysics 4.3b can be found in [20]. Model parameter values are:  $a=1425\text{A/m}$ ,  $\alpha=0.0005$ ,  $c=0.1$ ,  $k=255\text{A/m}$  and  $M_s=1\,500\,000\text{A/m}$ , i.e. the model is frequency-dependent.

### Potential formulations

Nowadays, there are many potential formulations for electromagnetic field calculation. The aim of using these formulations is to convert the Maxwell's equations to the

solution of partial differential equations with boundary conditions [1, 2].

Eddy currents have been neglected, i.e. the Maxwell's equations of quasi static magnetic field by differential form has been used:

$$(9) \text{curl } \mathbf{H} = \mathbf{J},$$

$$(10) \text{div } \mathbf{B} = 0,$$

where  $\mathbf{J}$  is the electric current density.

The first constitution relation is the same as (1). Introducing the magnetic vector potential  $A$ , using the identity of  $\text{divot}A = 0$  on (9) and (10) gives

$$(11) \mathbf{B} = \text{curl } \mathbf{A},$$

$$(12) \mathbf{H} = \frac{1}{\mu} \text{curl } \mathbf{A},$$

which lead to

$$(13) \text{curl } \frac{1}{\mu} \text{curl } \mathbf{A} = \mathbf{J}_0,$$

where  $\mathbf{J}_0$  is the source current density. The Neumann boundary condition on  $\Gamma_H$  is

$$(14) \frac{1}{\mu} \text{curl } \mathbf{A} \times \mathbf{n} = 0.$$

In (14)  $\mathbf{n}$  is the outer normal vector of the surface. The Dirichlet boundary condition on  $\Gamma_B$  is

$$(15) \mathbf{A} \times \mathbf{n} = 0.$$

In 2D problems Coulomb gauge  $\text{div}A = 0$  is satisfied automatically. The implementations of these equations into COMSOL was performed by using weak form of PDE. Ignoring the longer derivation, (16) is the result for air, (17) for coil and (18) for core domains when using nodal elements for approximation of  $A$

$$(16) \int_{\Omega} \frac{1}{\mu_0} \text{curl } \mathbf{W} \cdot \text{curl } \mathbf{A} \, d\Omega_0 = 0,$$

$$(17) \int_{\Omega_0} \frac{1}{\mu_0} \text{curl } \mathbf{W} \cdot \text{curl } \mathbf{A} \, d\Omega_0 = \int_{\Omega_0} \mathbf{W} \cdot \mathbf{J}_0 \, d\Omega_0,$$

$$(18) \int_{\Omega_m} \text{curl } \mathbf{W} \cdot \mathbf{H} \, d\Omega_m = 0.$$

### Implementation into COMSOL Multiphysics

COMSOL Multiphysics 4.3b has been chosen for simulation software. This version of the software does not have the built-in Jiles-Atherton model as the newer 5.2a version has [21]. The hysteresis model implementation has been published before [20]. Abandon the built-in magnetic field physics from the model means all the potential formulation equations must be added manually.

### 2D problem

The geometry of the Epstein frame is axial symmetrical, so the geometry can be simplified for a quarter [14]. The meshed geometry can be seen in Fig. 2, where  $\Omega_0$  is the air domain and  $\Omega_m$  shows the magnetic material where the Jiles-Atherton model is written on.

This geometry must be broken into two parts based on its magnetic behaviour, i.e. air and core. In the coil domains (17) can be applied, in the air part (16) can be used. This equation takes the following form in COMSOL:

$$(19) \frac{1}{\mu_0} (A1x \cdot \text{test}(A1x) + A1y \cdot \text{test}(A1y)).$$

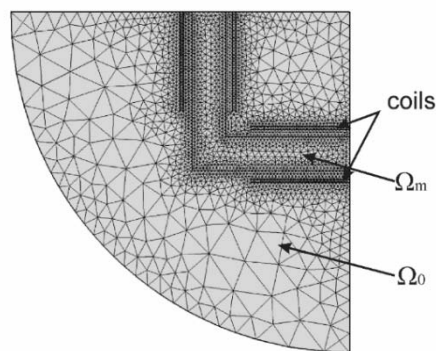


Fig. 1. The meshed 2D geometry in COMSOL Multiphysics

Equation (16) has been implemented as a weak form of PDE. The second -coil- part has been implemented as a weak contribution, where the current density  $\mathbf{J}_0$  can be determined as the product of the current and the surface. To validate (18) for the magnetic material, a separate PDE must be added because of the hysteresis model, where  $\mathbf{H}$  is the dependent variable of (8). (18) takes the following form in COMSOL:

$$(20) \text{test}(A1y) \cdot H1x - \text{test}(A1x) \cdot H1y.$$

### Simulation results

Simulations have been performed at 1Hz frequency with sinusoidal and current controlled excitation using the built-in modules and potential formalism. The time range of the time dependent solver has been set to 1.25 period with the number of values 101. Parallel Direct Sparse Solver (PARDISO) has been applied during the simulation with Newton's method for nonlinearity. The specification of the computer is the following: Intel Xeon E5-2670 v3, 32 vCPU and 32GB DDR4 RAM.

As it can be seen in Fig. 3. using sinusoidal current excitation there is maximum of 297A/m difference between the two curves. Applying formulation gives 3.17% higher magnetic field intensity  $\mathbf{H}$ . This difference is just the opposite when simulating with the control current (Fig. 4.). In this case, the maximum difference is 311A/m, but the formulation gives higher  $\mathbf{H}$ .

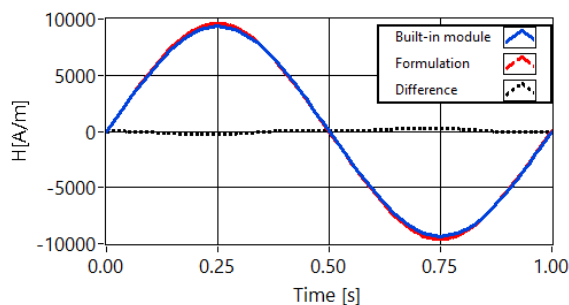


Fig. 2. Comparing magnetic field intensity  $\mathbf{H}$  using sinusoidal current excitation

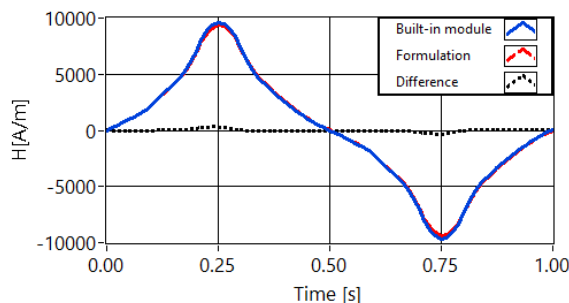


Fig. 3. Comparing magnetic field intensity  $\mathbf{H}$  using current controlled excitation

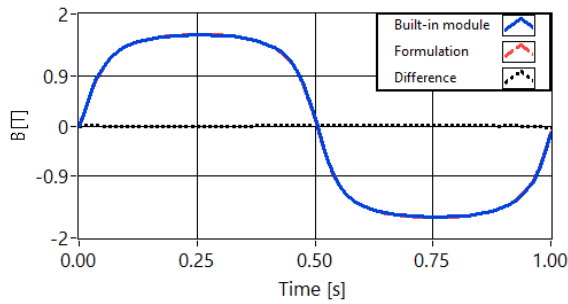


Fig.5. Comparing magnetic flux density  $B$  using sinusoidal current excitation

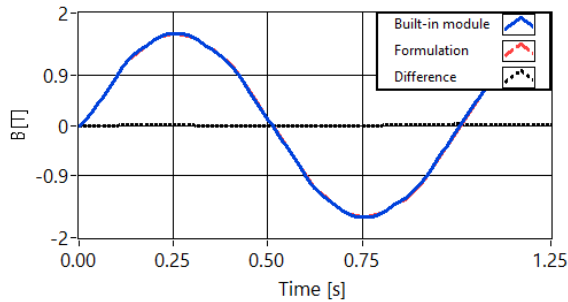


Fig.6. Comparing magnetic flux density  $B$  using current controlled excitation

Examining whether these excitation variations make a difference between magnetic flux density  $B$ , there is less than 1.43% difference between the results as it can be seen in Fig. 5. and Fig. 6.

The magnetization curves can be seen in Fig. 7. The difference between the curves negligible.

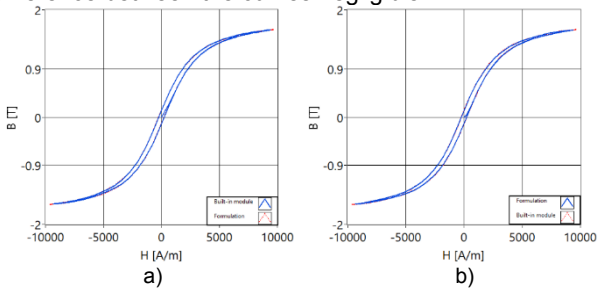


Fig.7. Magnetization curves with sinusoidal and current controlled excitation

The main goal was to reduce the software computational time while the accuracy should not decrease. This difference between the two techniques is acceptable, but the simulation time is longer than we expected even if the Degrees of Freedom (DOF) is reduced with 38%. Table 2 shows the simulation time with different methods.

Table 1. The parameters of the sensor

Method	Time [sec]	DOF
Built-in module with sinusoidal current	396	51244
Built-in module with controlled current	1309	51244
Formulation with sinusoidal current	17683	30032 (+1500 internal)
Formulation with controlled current	55039	30032 (+1500 internal)

### Power loss calculation

The power loss in magnetic materials can be calculated in different ways. For this work the solution has been chosen which one COMSOL also offers in the documentation [5]. In a linear material model, losses can be specified by the complex relative permeability

$$(21) \mu_r = \mu_r' + j\mu_r''$$

where  $\mu_r'$  represents the real part and  $\mu_r''$  is the imaginary part. The power density  $P_{\text{loss}}$  can be calculated by [5]

$$(22) P_{\text{loss}} = \omega \mu_0 \mu_r'' (\mathbf{H}_{\text{rms}} \cdot \mathbf{H}_{\text{rms}}),$$

where  $\mathbf{H}_{\text{rms}}$  is the root-mean-square value over one cycle. The power density can be calculated with an integration over time as well

$$(23) P_{\text{loss}} = \frac{1}{T} \int_0^T \left( \mathbf{H} \cdot \frac{\partial \mathbf{B}}{\partial t} \right) dt.$$

From (22) and (23) the following formulas can be deduced:

$$(24) \mathbf{B}_{\text{rms}} \cdot \mathbf{B}_{\text{rms}} = \mu_0^2 |\mu_r''|^2 (\mathbf{H}_{\text{rms}} \cdot \mathbf{H}_{\text{rms}}),$$

$$(25) \mu_r'' = \frac{1}{2\pi f \mu_0} \frac{\frac{1}{V_{\Omega_m}} \int_{\Omega_m} P_{\text{loss}} dV}{\frac{1}{V_{\Omega_m}} \int_{\Omega_m} \mathbf{H}_{\text{rms}} \cdot \mathbf{H}_{\text{rms}} dV},$$

$$(26) \mu_r' = \text{Re} \left\{ \sqrt{\frac{\frac{1}{V_{\Omega_m}} \int_{\Omega_m} (\mathbf{B}_{\text{rms}} \cdot \mathbf{B}_{\text{rms}}) dV}{\mu_0^2} - (\mu_r'')^2} \right\}.$$

Power loss simulation has been performed at 50Hz frequency. Sinusoidal current excitation has been used with the amplitude of 4.56A. The magnetization curve can be seen in Fig. 8.

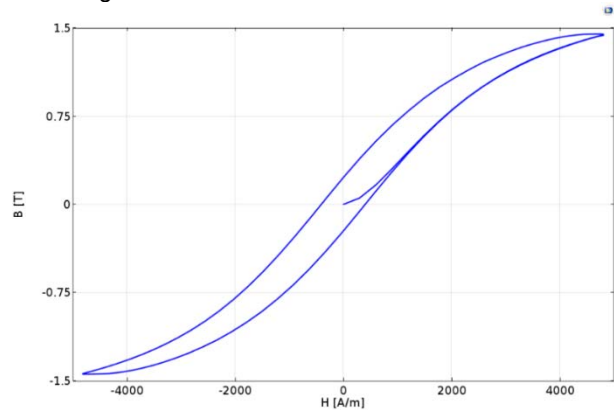


Fig.8. Magnetization curve performed at 50Hz frequency with sinusoidal current excitation

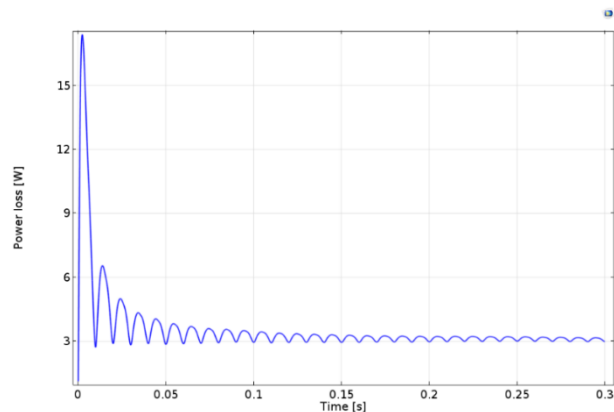


Fig.9. Power loss of the magnetic material on 50Hz frequency

After implementing equations (23)-(28), the power loss of the magnetic material can be calculated. The power loss simulation has been performed on 50Hz frequency because the catalogue values are also given at here. The simulation result can be seen in Fig. 9.

The catalogue value for loss on 50Hz at 1.4T magnetic flux density  $B$  is 2.00W/kg. The simulation gives 3.1W/kg after 15 period. The difference is large and can be caused by the physical impact, cutting, machining of the sample or by the damaged insulating coating.

## Conclusion

The test task is completed in which the Jiles-Atherton model has been implemented into COMSOL Multiphysics. The simulation results have been validated by measurements. Even if this 2D problem is quite simple compared to an induction machine, these results will be used later as the Jiles-Atherton model will be taken into account in induction machine LPV/qLPV modelling.

## Acknowledgement

Supported by EFOP-3.6.1-16-2016-00017:

*Internationalization, initiatives to establish a new source of researchers and graduates, and development of knowledge and technological transfer as instruments of intelligent specializations at Szechenyi University.*

**Authors:** Zoltan Németh, Department of Automation, Faculty of Mechanical Engineering, Informatics and Electrical Engineering, Széchenyi István University, Egyetem tér 1, H9026, Győr, Hungary, email: nemeth.zoltan@sze.hu; Prof. Miklós Kuczmann, Department of Automation, Faculty of Mechanical Engineering, Informatics and Electrical Engineering, Széchenyi István University, Egyetem tér 1, H9026, Győr, Hungary, email: kuczmann@sze.hu;

## REFERENCES

- [1] A. Ivanyi: Hysteresis models in electromagnetic computation, Academic press, Budapest, 1997.
- [2] A. Ivanyi, M. Kuczmann: The finite element method in magnetics, Academic press, Budapest, 2008.
- [3] A. Szollosi, P. Baranyi: Influence of the tensor product model representation of QLPV models on the feasibility of linear matrix inequality based stability analysis, *Asian Journal of control*, Vol. 20. No. 1, pp.531-547, 2018.
- [4] B. Koprivica, A. Milovanovic, V. Brkovic: Electrical steel testing using modified Epstein frame, *International Scientific Conference, Gabrovo*, 18-19 November 2016.
- [5] COMSOL: Modeling hysteresis effects, Solved with COMSOL Multiphysics 3.5a, 2008.
- [6] D. C. Jiles, D. L. Atherton: Ferromagnetic hysteresis, *IEEE Transaction on Magnetism*, Vol. 19, No. 5, pp. 2183–2185, 1983.
- [7] D. Jackiewicz, R. Szewczyk, J. Salach, A. Bienkowskyi: Application of Extended Jiles-Atherton model for modelling the influence of stresses on magnetic characteristics of the construction steel, *Acta Physica Polonica*, Vol. 125, No. 6, pp. 392-393, 2014.
- [8] D. Khamari, A. Makouf, S. Drid, C.A. Larbi: Robust Linear Parameter Varying Induction Motor Control with Polytopic Models, *Serbian Journal of Electrical Engineering*, Vol. 10, No. 2, pp. 335-348, June 2013.
- [9] D. Lin, P. Zhou, A. Bergqvist: Improved vector play model and parameter identification for magnetic hysteresis materials, *IEEE Transactions on Magnetism*, Vol. 50, No. 2, 2014.
- [10] G. Parent, R. Penin, J. P. Lecoq, J. F. Brundny, T. Belgrand: Determination of Specific Losses in the limbs of an Epstein frame using a three Epstein frame methodology applied to grain oriented electrical steels, *Sensors*, Vol. 16, No. 6, 826, 2016.
- [11] H. Benderradji, L. Chrifi-Alaoui, S. Mahieddine-Mahmoud, A. Makouf: Robust Control of Induction Motor with  $H^\infty$  Theory based on Loopshaping, *Journal of Electrical Engineering & Technology*, Vol. 6, No. 2, pp. 226-232, 2011.
- [12] IEC 60404-2 Magnetic materials, Part 2: Methods of measurement of the magnetic properties of electrical steel sheet and strip by means of an Epstein frame, International Electrotechnical Commission Std, 1996.
- [13] Ioan R. Ciric: Scalar potential formulations for magnetic fields produced by arbitrary electric current distributions on the presence of ferromagnetic bodies, *IEEE Transaction on Magnetism*, Vol. 50, No.1, 2014.
- [14] J. Bokor, P. Gáspár, Z. Szabó: Robust Control Theory with automotive applications, *Typotex*, 2012.
- [15] J. P.A. Bastos, N. Sadowski: Electromagnetic modeling by finite element methods, Marcel Dekker Inc, New York, 2003.
- [16] P. Baranyi: TP-model Transformation-Based-Control Design Frameworks, Springer International Publishing Switzerland, 2016.
- [17] P. Kis Jiles-Atherton model implementation to edge finite element method, PhD Thesis, Budapest University of Technology and Economics, 2007.
- [18] R. Kaczmarek, M. Amar, F. Protat: Iron loss under PWM voltage supply on Epstein frame and in induction motor core, *IEEE Transactions on Magnetism*, Vol. 32, No. 1, pp. 189-194, 1996.
- [19] S. M. Nawazish Ali, Athar Hanif, M. J. Hossain, Vivek Sharma: An LPV  $H^\infty$  Control Design for the Varying Rotor Resistance Effects on the Dynamic Performance of Induction Motors, *Industrial Electronics (ISIE) 2018 IEEE 27th International Symposium*, pp. 114-119, 2018.
- [20] Z. Németh, M. Kuczmann: Measuring and simulation magnetic characteristics using Epstein frame, *Pollack Periodica*, Vol. 13, No. 2, pp. 15-26 (2018).
- [21] COMSOL Multiphysics 5.2a Release highlights: <https://www.comsol.com/release/5.2a/acdc-module>